

Particle-based fluid dynamics: comparison of different Bhatnagar-Gross-Krook models and the Direct Simulation Monte Carlo method for hypersonic flows

M. Pfeiffer^{1, a)}

*Institute of Space Systems, University of Stuttgart, Pfaffenwaldring 29,
D-70569 Stuttgart, Germany*

(Dated: 2 October 2018)

The Bhatnagar-Gross-Krook (BGK) model as well as its extensions (ellipsoidal statistical BGK, Shakhov BGK, unified BGK) are used in particle-based fluid dynamics and compared with the Direct Simulation Monte Carlo (DSMC) method. To this end, different methods are investigated that allow efficient sampling of the Shakhov and the unified target distribution functions. As a consequence, particle simulations based on the Shakhov BGK and the unified BGK model are possible in an efficient way. Furthermore, different energy conservation schemes are tested for the BGK models. It is shown that the choice of the energy conservation scheme has a major impact on the quality of the results for each model. The models are verified with a Couette flow problem at different Knudsen numbers and wall velocities. Furthermore, the models are compared with DSMC results of a hypersonic flow around a 70° blunted cone. It is shown that the unified BGK model is able to reproduce rarefied gas phenomena. Furthermore, it is shown that the difference in the reproduction of shock structure is not significant between the ellipsoidal statistical BGK and Shakhov BGK model for the flow around a 70° blunted cone and significantly depends on the energy conservation method. The choice of the energy conservation method is especially crucial for the Shakhov model whereas the ellipsoidal statistical BGK model is much more robust concerning the energy conservation scheme. Additionally, a computational time study is done to show the efficiency of BGK-based simulations for low Knudsen number flows compared with DSMC.

Keywords: DSMC, Shakhov, Ellipsoidal statistical BGK, BGK

^{a)}Electronic mail: mpfeiffer@irs.uni-stuttgart.de

I. INTRODUCTION

Simulations of gas flows which cover a wide range of Knudsen numbers including continuum and rarefied gas regions are still challenging. CFD methods based on Navier-Stokes equations cover a wide range of near equilibrium flows that are important for many practical applications. Nevertheless, the assumptions behind the Navier-Stokes equations become invalid for rarefied non-equilibrium flows. For this purpose, the Direct Simulation Monte Carlo (DSMC) method can be used to treat non-equilibrium effects in rarefied gases¹. Therefore, the collision integral is not solved directly. Consequently, the DSMC method becomes very expensive for small Knudsen number flows due to the fact that molecular events must be spatially- and time-resolved within the mean free path and collision frequency scales, respectively. To close the gap between the applicable regimes of both methods, different approaches are used.

A straightforward approach to overcome this gap is the coupling of DSMC with CFD. Here, many problems arise due to the very different underlying approaches of both methods. Especially the statistical noise of the DSMC method is problematic at the boundaries between DSMC and CFD. Another possibility are particle-based continuum methods, which can be easily coupled with DSMC. A variety of different methods were introduced in the past, e.g. the Time Relaxed Monte Carlo method², the Viscous Collision Limiter method³, the Fokker-Planck solution algorithm^{4,5}, the low diffusion method^{6,7} and more. A short overview with advantages and disadvantages of these methods is given in Mirza et al.⁷.

Another particle method that is already used and coupled to DSMC in different applications like nozzle flow expansion⁸, micro channel flows (MEMS) simulations⁹ or simulations of hypersonic shocks¹⁰ is the statistical Bhatnagar-Gross-Krook (BGK) method. Up to now, only the ellipsoidal statistical BGK (ESBGK) model has been used in this context. Unfortunately, the ESBGK model has difficulties to reproduce the shock structure correctly¹¹. In this publication, methods to sample in an efficient way from other target distribution functions used in the Shakhov and unified BGK models are described. Furthermore, different energy and momentum conservation schemes are investigated, which are especially critical for the Shakhov model to achieve a correct physical behavior. Finally, different BGK models (BGK, ESBGK, Shakhov BGK, Unified BGK) will be verified by simulating Couette flow problems and tested as well as compared concerning the reproduction of hypersonic shocks.

II. THEORY

The Boltzmann equation fully describes the behavior of a monoatomic gas with the corresponding distribution function $f = f(\mathbf{x}, \mathbf{v}, t)$ at position \mathbf{x} and velocity \mathbf{v}

$$\frac{\partial f}{\partial t} + \mathbf{v} \frac{\partial f}{\partial \mathbf{x}} = \frac{\partial f}{\partial t} \Big|_{Coll}. \quad (1)$$

In this equation, external forces are neglected. Furthermore, $\partial f / \partial t|_{Coll}$ is the collision term, which can be described by the Boltzmann collision integral

$$\frac{\partial f}{\partial t} \Big|_{Coll} = \int_{\mathbb{R}^3} \int_{S^2} \mathcal{B} [f(\mathbf{v}')f(\mathbf{v}'_*) - f(\mathbf{v})f(\mathbf{v}_*)] d\mathbf{n}d\mathbf{v}_*. \quad (2)$$

Here, $S^2 \subset \mathbb{R}^3$ is the unit sphere, \mathbf{n} is the unit vector of the scattered velocities, \mathcal{B} is the collision kernel and the superscript ' denotes the post collision velocities. The multiple integration of this collision term makes it difficult to compute in the 6D phase space.

A. BGK Models

The BGK model approximates the collision term to a simple relaxation form where the distribution function relaxes towards a target distribution function f^t with a certain relaxation frequency ν :

$$\frac{\partial f}{\partial t} \Big|_{Coll} = \nu (f^t - f). \quad (3)$$

The original BGK model assumes, that the target velocity distribution function is the Maxwellian velocity distribution f^M

$$f^M = n \left(\frac{m}{2\pi k_B T} \right)^{3/2} \exp \left[-\frac{m\mathbf{c}^2}{2k_B T} \right], \quad (4)$$

with the particle density n , particle mass m , temperature T , Boltzmann constant k_B and the thermal particle velocity $\mathbf{c} = \mathbf{v} - \mathbf{u}$ from the particle velocity \mathbf{v} and the average flow velocity \mathbf{u} ¹². The BGK model reproduces the Maxwellian distribution in an equilibrium state, preserves conservation of mass, momentum and energy as well as fulfills the H-theorem¹³.

The relaxation frequency ν defines the viscosity μ and the thermal conductivity K

$$\mu = \frac{nk_B T}{\nu} \quad K = \frac{c_P n k_B T}{\nu} \quad (5)$$

with the specific heat constant $c_P = 5k_B/2m$. These equations clarify the problem of the BGK model concerning the Prandtl number, which is fixed in this model to $Pr = \mu c_P / K =$

1, whereas the Prandtl number of monoatomic gases is $Pr \approx 2/3^{14}$. As a consequence, only the thermal conductivity or viscosity can be correctly reproduced at a time with the BGK model. To overcome this problem, several extensions of the BGK model were introduced in the past. Some of these models transform the target distribution function e.g. the ellipsoidal statistical BGK model¹⁵ or the Shakhov BGK model¹⁶, other models change the relaxation frequency from a constant to a function of the microscopic velocities as described in Struchtrup¹⁷. In this paper, only models with a transformed target distribution are investigated.

1. *Ellipsoidal Statistical BGK Model*

The ellipsoidal statistical BGK (ESBGK) model replaces the Maxwellian target distribution of the standard BGK model with an anisotropic Gaussian distribution¹³

$$f^{ES} = \frac{n}{\sqrt{\det \mathcal{A}}} \left(\frac{m}{2\pi k_B T} \right)^{3/2} \exp \left[-\frac{m \mathbf{c}^T \mathcal{A}^{-1} \mathbf{c}}{2k_B T} \right] \quad (6)$$

with the anisotropic matrix

$$\mathcal{A} = \mathcal{I} - \frac{1 - Pr}{Pr} \left(\frac{3\mathcal{P}}{\text{Tr}[\mathcal{P}]} - \mathcal{I} \right). \quad (7)$$

The anisotropic matrix \mathcal{A} consists of the identity matrix \mathcal{I} and the pressure tensor \mathcal{P}

$$\mathcal{P} = \int \mathbf{c} \mathbf{c}^T f d\mathbf{v}, \quad (8)$$

which are both symmetric. The ESBGK model reproduces the Maxwellian distribution in the equilibrium state as well as the correct moments of the Boltzmann equation. Furthermore, Andries et al.^{18,19} have shown that it fulfills the H-theorem. In the ESBGK model, the viscosity and the thermal conductivity are defined as

$$\mu = \frac{nk_B T}{\nu} Pr \quad K = \frac{c_P nk_B T}{\nu}. \quad (9)$$

Due to the fact that the viscosity depends on the Prandtl number, it is now possible to reproduce the viscosity and thermal conductivity at the same time. So, the introduction of the Prandtl number as an additional parameter resolves the Prandtl number problem of the standard BGK model.

As proposed by Gallis and Torczynski¹³, a symmetric transformation matrix \mathcal{S} with $\mathcal{A} = \mathcal{S}\mathcal{S}$ can be defined. Furthermore, a normalized thermal velocity vector \mathbf{C} is defined

such that $\mathbf{c} = \mathcal{S}\mathbf{C}$. Using these definitions, the argument of the exponential function in Eq. (6) becomes

$$\mathbf{c}^T \mathcal{A}^{-1} \mathbf{c} = (\mathcal{S}\mathbf{C})^T \mathcal{S}^{-1} \mathcal{S}^{-1} \mathcal{S}\mathbf{C} = \mathbf{C}^T \mathbf{C} \quad (10)$$

using $(\mathcal{S}\mathbf{C})^T = \mathbf{C}^T \mathcal{S}^T = \mathbf{C}^T \mathcal{S}$ due to the fact that \mathcal{S} is symmetric. So, \mathcal{S} can transform a vector \mathbf{C} sampled from a Maxwellian distribution to a vector \mathbf{c} sampled from Eq. (6).

2. *Shakhov BGK Model*

In contrast to the ESBGK model, which modifies the shear stress to produce the correct Prandtl number²⁰, the Shakhov model (SBGK) directly modifies the heat flux. For this, the target distribution of the BGK model is changed to

$$f^S = f^M \left[1 + (1 - Pr) \frac{\mathbf{c}\mathbf{q}}{5n(RT)^2} \left(\frac{\mathbf{c}^2}{2RT} - \frac{5}{2} \right) \right] \quad (11)$$

with the heat flux vector

$$\mathbf{q} = \int \mathbf{c}\mathbf{c}^2 f d\mathbf{v}, \quad (12)$$

and the specific gas constant R . In the SBGK model, the viscosity and the thermal conductivity are defined as

$$\mu = \frac{nk_B T}{\nu} \quad K = \frac{c_P n k_B T}{\nu} \frac{1}{Pr}. \quad (13)$$

Consequently, this model solves the Prandtl number problem of the original BGK model and reproduces the Maxwellian distribution in the equilibrium state as well as the correct moments of the Boltzmann equation. The main disadvantage of the SBGK model compared to the ESBGK model is that no general proof exists whether the SBGK model always fulfills the H-theorem. Furthermore, it cannot be guaranteed that f^S is positive in each situation²⁰.

3. *Unified BGK Model*

Chen et al.¹¹ proposed a unified BGK model (UBGK), which merges the ESBGK and SBGK model. The new target distribution is

$$f^U = f^{ES*} + f^{S*} \quad (14)$$

$$f^{ES*} = \frac{n}{\sqrt{\det \mathcal{A}^*}} \left(\frac{m}{2\pi k_B T} \right)^{3/2} \exp \left[-\frac{m \mathbf{c}^T \mathcal{A}^{*-1} \mathbf{c}}{2k_B T} \right] \quad (15)$$

$$\mathcal{A}^* = \mathcal{I} + C_{ES} \left(\frac{3\mathcal{P}}{\text{Tr}[\mathcal{P}]} - \mathcal{I} \right) \quad (16)$$

$$f^{S*} = f^M (1 - C_S) \frac{\mathbf{c}\mathbf{q}}{5n(RT)^2} \left(\frac{\mathbf{c}^2}{2RT} - \frac{5}{2} \right). \quad (17)$$

The UBGK model depends on two different parameters C_{ES} and C_S with

$$Pr = \frac{C_S}{1 - C_{ES}}. \quad (18)$$

Therefore, this model introduces an additional independent parameter for a derived Prandtl number. This parameter can basically be chosen freely but the ES model constrains C_{ES} to the interval $[-0.5, 1)$ to preserve positive eigenvalues of \mathcal{A}^{11} . When $C_{ES} = 0$ and $C_S = Pr$ the UBGK model reduces to the Shakhov model. On the other hand, if $C_{ES} = 1 - 1/Pr$ and $C_S = 1$ the UBGK model is identical to the ESBGK model. For other values, the UBGK model blends the ESBGK and Shakhov model. The viscosity and the thermal conductivity for the UBGK model are defined as

$$\mu = \frac{nk_B T}{\nu(1 - C_{ES})} \quad K = \frac{c_P n k_B T}{\nu} \frac{1}{C_S}. \quad (19)$$

Finally, the UBGK model allows to modify the shear stress as well as the heat flux at once. Or with other words, the parameters C_{ES} and C_S can be used to determine different relaxation rates of \mathcal{P} and \mathbf{q} ²⁰:

$$\frac{\partial \mathcal{P}}{\partial t} = \frac{-(1 - C_{ES})}{\nu} \mathcal{P}, \quad \frac{\partial \mathbf{q}}{\partial t} = \frac{-C_S}{\nu} \mathbf{q}. \quad (20)$$

The problem of the UBGK model is that it is not clear how C_{ES} and C_S should be chosen. Chen et al.¹¹ exemplary show that when C_S is used to produce the right Prandtl number, C_{ES} can be derived as

$$C_{ES}^{VHS} = 1 - \frac{(7 - 2\omega)(5 - 2\omega)}{30}, \quad (21)$$

for VHS molecules with the VHS parameter ω in an equilibrium state. However, they also showed that C_{ES} totally differs for non-equilibrium states.

III. IMPLEMENTATION

The different BGK models are implemented in the PIC-DSMC code PICLas²¹ and verified by the comparison to DSMC results of PICLas. The DSMC method is widely used and details can be found in Bird¹.

For the BGK models, the statistic particle method of Gallis and Torczynski^{13,22} is used. Here, particles are moved in a simulation mesh, collide with boundaries and microscopic particle properties are sampled to calculate macroscopic values in the same manner as in DSMC. But in contrast to the DSMC method, the collision step with binary collisions between the particles is not performed. Instead, each particle in a cell relaxes with the probability

$$P = 1 - \exp[-\nu\Delta t] \quad (22)$$

according to Eq. (3) towards the target distribution. The relaxation frequency ν is evaluated in each time step for each cell from the definition of the viscosity of each model. The relaxation frequency directly depends on the cell temperature T , which is calculated from the particle information. For the viscosity μ the well known exponential ansatz

$$\mu = \mu_{ref} \left(\frac{T}{T_{ref}} \right)^\omega \quad (23)$$

is used. Here, T_{ref} is a reference temperature and μ_{ref} the reference dynamic viscosity at T_{ref} ⁸. For a VHS gas the reference dynamic viscosity can be calculated with the VHS reference diameter d_{ref} of the particles:

$$\mu_{ref} = \frac{30\sqrt{mk_B T_{ref}}}{\sqrt{\pi}4(5-2\omega)(7-2\omega)d_{ref}^2}. \quad (24)$$

If a particle is chosen to relax, the new particle velocity is sampled from the target distribution.

A. Energy and Momentum Conservation

To conserve momentum and energy, two different methods are proposed in the literature. In the method of Gallis and Torczynski¹³, the average velocity and the temperature for each particle N in a cell are determined before the collision (\mathbf{u} and T) and for the provisional

post collision conditions (\mathbf{u}_p and T_p):

$$\mathbf{u} = \frac{1}{N} \sum_{i=1}^N \mathbf{v}_i \quad (25)$$

$$T = \frac{1}{N-1} \sum_{i=1}^N \frac{m\mathbf{v}_i^2}{3k_B}. \quad (26)$$

The factor $\frac{1}{N-1}$ in the temperature occurs to produce unbiasedness of T^{23} . The final post-collision velocity \mathbf{v}^* of every molecule (whether having undergone relaxation or not) is then determined from the provisional postcollision velocity \mathbf{v}_p according to

$$\mathbf{v}^* = \mathbf{u} + (\mathbf{v}_p - \mathbf{u}_p) \sqrt{\frac{T}{T_p}}. \quad (27)$$

In the method of Burt and Boyd⁸, the same guarantee is performed but only with N_{relax} particles that take part in the relaxation process whereas all other particles will remain unaffected. Obviously, this method can only be performed if at least two particles are chosen to relax. To handle the case $N_{relax} = 1$, a random number is used to decide whether $N_{relax} = 0$ or $N_{relax} = 2$ with equal probability. If N_{relax} is determined to two, the second particle is chosen randomly from the remaining not relaxing particles.

B. Relaxation Process

In the standard BGK collision term, the postcollision velocities \mathbf{v}_p are simply sampled from the Maxwellian distribution (4)

$$\mathbf{v}_p = \boldsymbol{\xi} \sigma_T, \quad (28)$$

with the normal distributed random vector $\boldsymbol{\xi}$ and the velocity $\sigma_T = \sqrt{k_B T/m}$.

1. Sampling from *ESBGK*

The sampling from the *ESBGK* distribution in Eq. (6) is performed with three different approaches.

In the first approach an approximation of the transformation matrix \mathcal{S} of Eq. (10) is used as described in previous studies^{8,10,13}

$$\mathcal{S}_{ij} = \delta_{ij} - \frac{1 - Pr}{2Pr} \left[\frac{m}{k_B T} \frac{N}{N-1} (\mathcal{P}_{ij} - \hat{c}_i \hat{c}_j) - \delta_{ij} \right] \quad (29)$$

with

$$\hat{\mathbf{c}} = \int \mathbf{c} f d\mathbf{v}. \quad (30)$$

The advantage of this approach is that this method is fast and simple to implement. Nevertheless, the accuracy and performance of this approximation has to be tested.

The second approach is the exact calculation of \mathcal{S} by solving $\mathcal{A} = \mathcal{S}\mathcal{S}$ to find the square root of \mathcal{A} . For this, the matrix \mathcal{A} is diagonalized to the form

$$\mathcal{A} = \mathcal{V}\mathcal{D}\mathcal{V}^T. \quad (31)$$

The columns of \mathcal{V} are the eigenvectors of \mathcal{A} and the diagonal elements of the diagonal matrix \mathcal{D} are the corresponding eigenvalues. The square root of \mathcal{A} can now be calculated with

$$\mathcal{S} = \mathcal{V}\mathcal{D}^{1/2}\mathcal{V}^T, \quad (32)$$

where the diagonal elements of the diagonal matrix $\mathcal{D}^{1/2}$ are the square roots of the eigenvalues.

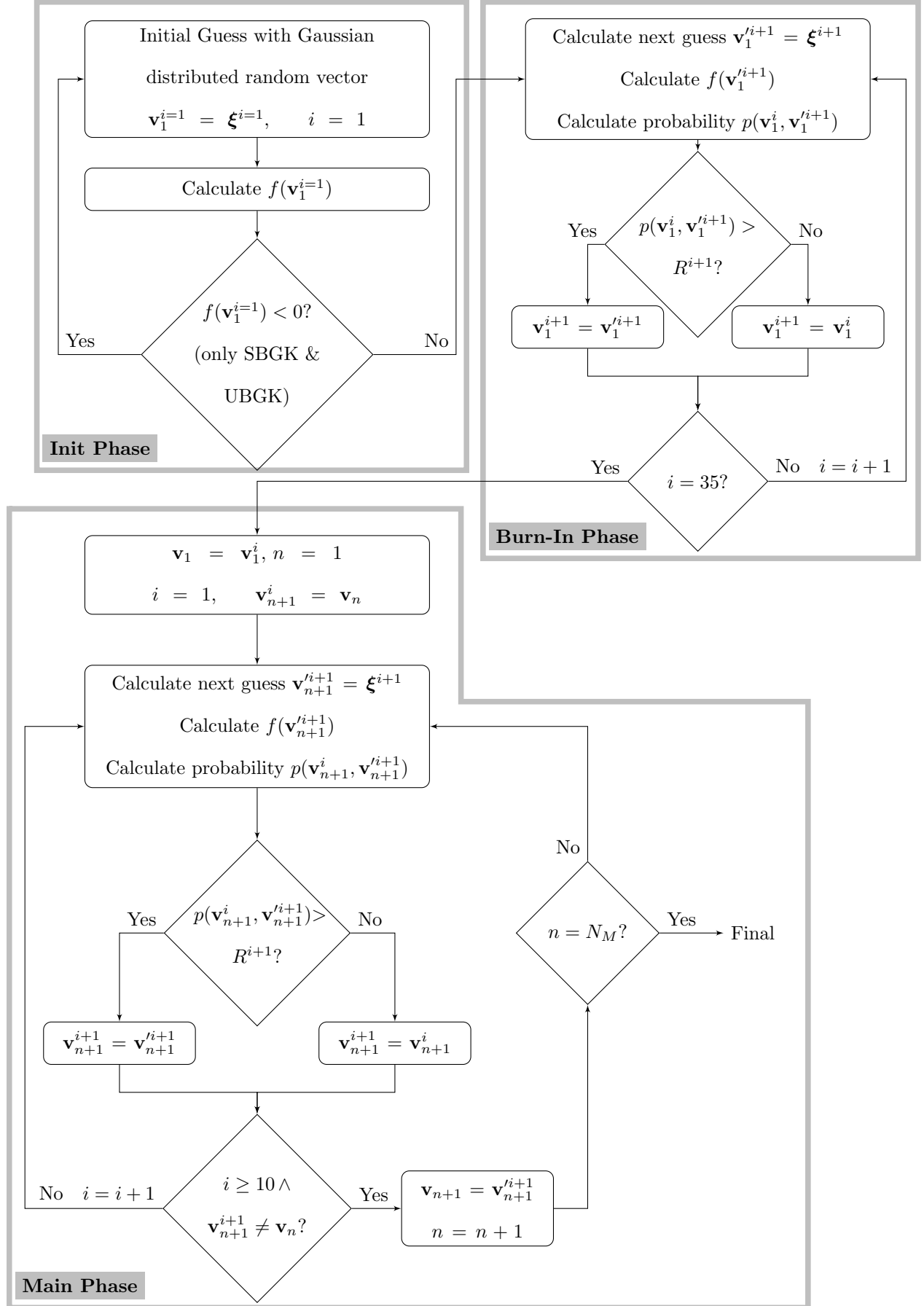
Metropolis-Hastings Sampling

The third approach is the direct sampling from f^{ES} by using a Metropolis-Hastings method which produces a Markov chain $\mathbf{v}_0, \mathbf{v}_1, \dots, \mathbf{v}_{N_M}$ of samples from the target distribution²⁴⁻²⁷. The MH method has the advantage that the determination of the global maximum of the target distribution function, which can be computationally expensive (e.g. for the proposed SBGK and UBGK distribution function), or the definition of an envelope function is not necessary in contrast to the acceptance-rejection (AR) method.

Starting with a sample \mathbf{v}_n , a proposed sample \mathbf{v}'_{n+1} is generated using a pre-specified density $q(\mathbf{v}_n, \mathbf{v}'_{n+1})$ and accepted as the next sample \mathbf{v}_{n+1} of the Markov chain with the probability

$$p(\mathbf{v}_n, \mathbf{v}'_{n+1}) = \begin{cases} \min\left(1, \frac{f(\mathbf{v}'_{n+1})q(\mathbf{v}_{n+1}, \mathbf{v}_n)}{f(\mathbf{v}_n)q(\mathbf{v}_n, \mathbf{v}'_{n+1})}\right), & f(\mathbf{v}_n)q(\mathbf{v}_n, \mathbf{v}'_{n+1}) > 0 \\ 1, & f(\mathbf{v}_n)q(\mathbf{v}_n, \mathbf{v}'_{n+1}) = 0. \end{cases} \quad (33)$$

If the proposed value \mathbf{v}'_{n+1} is not accepted, the next step of the Markov chain is set to $\mathbf{v}_{n+1} = \mathbf{v}_n$. A special case of the Metropolis-Hastings method (MH) is the random-walk Metropolis



algorithm. Here, q is a symmetrical function about zero, $q(\mathbf{v}_n, \mathbf{v}'_{n+1}) = q(\mathbf{v}'_{n+1}, \mathbf{v}_n)$ and the probability in Eq. (33) simplifies to

$$p(\mathbf{v}_n, \mathbf{v}'_{n+1}) = \min \left(1, \frac{f(\mathbf{v}'_{n+1})}{f(\mathbf{v}_n)} \right). \quad (34)$$

For the sampling from f^{ES} , q is chosen as a Gaussian distribution, which is symmetric. The detailed flowchart of the used MH algorithm is shown in Fig. 1. First, the initial phase is used to find a proper start value of the MH algorithm. The start value is chosen with

$$\mathbf{v}_1 = \boldsymbol{\xi} \quad (35)$$

and the normal distributed random vector $\boldsymbol{\xi}$. Next, the distribution function $f(\mathbf{v}_1)$ is calculated to check whether $f(\mathbf{v}_1)$ is positive. This step is not necessary for the ESBGK distribution function but if the used target distribution function does not fulfill the positivity requirements for probabilities (e.g. the case for SBGK and UBGK), these samples must be discarded. Therefore, another normal distributed random vector $\boldsymbol{\xi}$ is used until $f(\mathbf{v}_1) > 0$. A positive effect of the described MH algorithm is that if the first sample \mathbf{v}_1 fulfills $f(\mathbf{v}_1) > 0$, then also all following samples will fulfill this condition. Due to the fact that $p(\mathbf{v}_n, \mathbf{v}'_{n+1})$ would have to become negative, such samples cannot be chosen anymore.

The next proposed value is determined using again a new normal distributed random vector $\boldsymbol{\xi}$:

$$\mathbf{v}'_{n+1} = \boldsymbol{\xi} \quad (36)$$

A characteristic of the MH algorithm is the so called *burn-in* phase, which means that the first samples may not necessarily follow the target distribution, especially if the starting point is in a region of low density. Therefore, samples made during the *burn-in* phase have to be discarded. Different simulations have shown that 35 initial steps are sufficient to overcome the *burn-in* phase, before the first velocity is accepted. For each following final accepted velocity in the main phase, the velocity should be changed at least one time and at least 10 steps in the Markov chain should be taken. Note, that the *burn-in* phase must be done in each cell every time step due to the changed target distribution.

For the ESBGK method, the probability $p(\mathbf{v}_n, \mathbf{v}'_{n+1})$ is

$$p^{ESBGK}(\mathbf{v}_n, \mathbf{v}'_{n+1}) = \min \left(1, \frac{\exp[-0.5\mathbf{v}'_{n+1}{}^T \mathcal{A}^{-1} \mathbf{v}'_{n+1}]}{\exp[-0.5\mathbf{v}_n{}^T \mathcal{A}^{-1} \mathbf{v}_n]} \right) \quad (37)$$

The final postcollision velocities are obtained by scaling the sampled velocities

$$\mathbf{v}_{n,p} = \mathbf{v}_n \sigma_T. \quad (38)$$

2. Sampling from SBGK

In contrast to the ESBGK model, an analytical expression to convert a normal distributed vector in a SBGK distributed vector is not available (see Eq. (29)). Therefore, the SBGK distribution is sampled using two different methods. The first method is the already mentioned MH algorithm.

For this, almost the same algorithm as for the ESBGK MH sampling is used, including the start and proposed velocities, the *burn-in* phase as well as the final scaling of the velocities (see Sec. III A for energy conservation details). The probability in Eq. (34) is changed to

$$p^{SBGK}(\mathbf{v}_n, \mathbf{v}'_{n+1}) = \min \left(1, \frac{\left(1 + (1 - Pr) \frac{\mathbf{v}'_{n+1} \mathbf{q}}{5n\sigma_T^{3/2}} \left(\frac{\mathbf{v}'_{n+1}{}^2}{2} - \frac{5}{2} \right) \right)}{\left(1 + (1 - Pr) \frac{\mathbf{v}_n \mathbf{q}}{5n\sigma_T^{3/2}} \left(\frac{\mathbf{v}_n^2}{2} - \frac{5}{2} \right) \right)} \right). \quad (39)$$

Note that unbiasedness of the heat flux vector from Eq. (12) can be achieved using

$$\mathbf{q} = n \frac{N}{(N-1)(N-2)} \sum_{i=1}^N \mathbf{c}_i \mathbf{c}_i^2. \quad (40)$$

Instead of the MH method also the acceptance-rejection method can be used to sample from the Shakhov model. As shown for the Chapman-Enskog distribution in Garica and Alder²⁷, an envelope function $g(\boldsymbol{\xi})$ must be defined with $g(\boldsymbol{\xi}) \geq f^S(\boldsymbol{\xi})$ for all $\boldsymbol{\xi}$. A detailed description how $g(\boldsymbol{\xi})$ should be defined can be found in Garica and Alder²⁷. However, good results for the following test cases are found for $g(\boldsymbol{\xi}) = Af^M(\boldsymbol{\xi})$ with

$$A = 1 + 4 \max \left(\frac{|q_j|}{\sigma_T^{3/2}} \right), \quad j = 1, 2, 3. \quad (41)$$

The single steps for the acceptance-rejection sampling are:

1. Calculate A
2. Draw a normal distributed $\mathbf{v}_n = \boldsymbol{\xi}$
3. Accept \mathbf{v}_n if random number $R < p^{SBGK, AR}(\mathbf{v}_n)/A$

4. Calculate $v_{n,p} = \mathbf{v}_n \sigma_T$

$$\text{with } p^{SBGK,AR}(\mathbf{v}_n) = \left(1 + (1 - Pr) \frac{\mathbf{v}_n \mathbf{q}}{5n\sigma_T^{3/2}} \left(\frac{\mathbf{v}_n^2}{2} - \frac{5}{2} \right) \right).$$

3. Sampling from UBGK

The UBGK distribution is again sampled using the MH algorithm. As in the case of the SBGK sampling, only the probability in Eq. (34) is changed

$$p^{UBGK}(\mathbf{v}_n, \mathbf{v}'_{n+1}) = \min \left(1, \frac{\hat{p}^{UBGK,1}(\mathbf{v}'_{n+1}) + \hat{p}^{UBGK,2}(\mathbf{v}'_{n+1})}{\hat{p}^{UBGK,1}(\mathbf{v}_n) + \hat{p}^{UBGK,2}(\mathbf{v}_n)} \right), \quad (42)$$

$$\hat{p}^{UBGK,1}(\mathbf{x}) = \exp [-0.5\mathbf{x}^T \mathcal{A}^{-1} \mathbf{x}], \quad (43)$$

$$\hat{p}^{UBGK,2}(\mathbf{x}) = \exp [-0.5\mathbf{x}^2] \left((1 - Pr) \frac{\mathbf{x} \mathbf{q}}{5n\sigma_T^{3/2}} \left(\frac{\mathbf{x}^2}{2} - \frac{5}{2} \right) \right). \quad (44)$$

The UBGK method is not sampled using the acceptance-rejection method, due to the fact that the definition of the envelope function is cumbersome.

Note that the Metropolis-Hastings algorithm described here can be basically used to sample efficiently from an arbitrary target distribution and is not limited to the ESBGK, SBGK and the UBGK target distributions.

IV. SIMULATION RESULTS

A. Couette Flow

The first test case is a steady planar Couette flow of Argon similar to Kumar et al.²⁸. For this, two parallel plates form a channel and move in opposite directions with a velocity v_{Wall} . All other boundaries are periodic, resulting in a 1D test case. The distance between the plates is $D = 1$ m. The simulations are performed with 100 grid cells between the plates. The DSMC solver in PICLas additionally uses an octree method²⁹. Therefore, each cell is subdivided to resolve the mean free path of the particles. The BGK methods are performed on the same mesh but without a mesh adaptation in this test case.

The used Argon parameters are $d_{ref} = 4.17 \cdot 10^{-10}$ m, $T_{ref} = 273$ K, $\omega_{VHS} = 0.81$ and $m = 6.631368 \cdot 10^{-26}$ kg. The initial gas temperature as well as the temperature of the plates is in each simulation $T_{Wall} = 273$ K. Additionally, diffuse reflection with full accommodation is assumed on the plates.

Comparison of DSMC and particle based BGK models

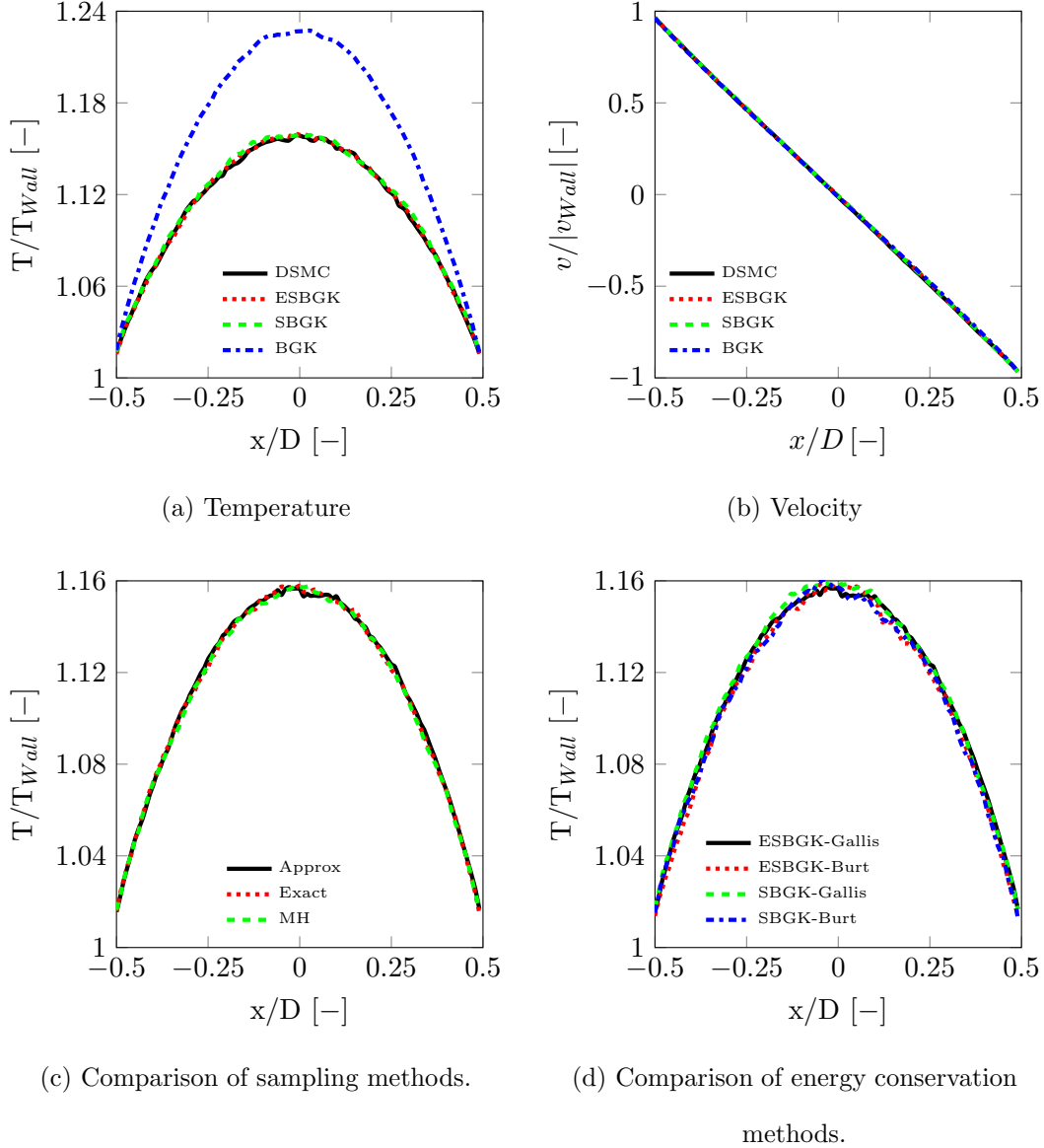


FIG. 2. Simulation results for the low wall velocity case ($Kn \approx 0.014$, $v_{Wall} = \pm 250$ m/s): (a) temperature profiles and (b) velocity profiles using different BGK models. (c) Comparison of ESBGK sampling methods. (d) Comparison of energy conservation methods.

1. Low Wall Velocity Case - $Kn \approx 0.014$

In the low velocity case, the plate velocity is $v_{Wall} = \pm 250$ m/s and the particle density is $n = 1.29438 \cdot 10^{20}$ 1/m³. This leads to a Knudsen number of $Kn \approx 0.014$. The results of the temperature and velocity profiles between the plates for the different methods are shown in Fig. 2a and 2b. The ESBGK as well as the SBGK method match the DSMC results very well whereas a clear difference is visible in the temperature plot for the BGK method.

Comparison of DSMC and particle based BGK models

Model	ESBGK	ESBGK	ESBGK	SBGK	SBGK	BGK*	UBGK
	Appr.	Exact	MH	MH	AR		MH
	$C_{ES} = 0.1$						
CPU time [s] per 1000 iterations	78	78	83	83	82	75	94

TABLE I. CPU time of different models all simulated on one core. * The BGK method does not need a special sampling since only normal distributed random numbers are necessary. The normal distributed random numbers for all simulations are generated using the Ziggurat algorithm³⁰.

Additionally, the three different methods of sampling from the ESBGK distribution (see Sec. III B 1) are compared. Fig. 2c shows that there is no visible difference in the temperature plot. Furthermore, the energy conservation schemes described in Sec. III A are compared in Fig. 2d. Here again no significant difference between the energy conservation schemes can be found. Therefore all other Couette flow simulations are done using only the energy conservation scheme of Gallis and Torczynski¹³. Nevertheless, it is shown later that the energy conservation scheme becomes significant in reproducing the correct heat flux values in hypersonic flows including shocks. Finally, the computational time of the different methods is compared in Table I, showing that there is no significant difference using the different models.

2. High Wall Velocity Case - $Kn \approx 0.014$

The high velocity case has a plate velocity of $v_{wall} = \pm 750$ m/s and a particle density of $n = 1.29438 \cdot 10^{20}$ 1/m³. So, the Knudsen number is again $Kn \approx 0.014$. The results of this case for the temperature and velocity profiles between the plates are shown in Fig. 3a and 3b. As in the case of the low wall velocity, the ESBGK as well as the SBGK match the DSMC result very well whereas the BGK model overestimates the temperature. Furthermore, the UBGK model was tested with this case. The results compared with the DSMC method are shown in Fig. 3c and 3d. The temperature overestimates the DSMC result for the VHS equilibrium solution of $C_{ES} \approx 0.4$ (Eq. (21)). For decreasing C_{ES} , the UBGK temperature approaches the DSMC temperature. Clearly, the UBGK method would match the DSMC

Comparison of DSMC and particle based BGK models

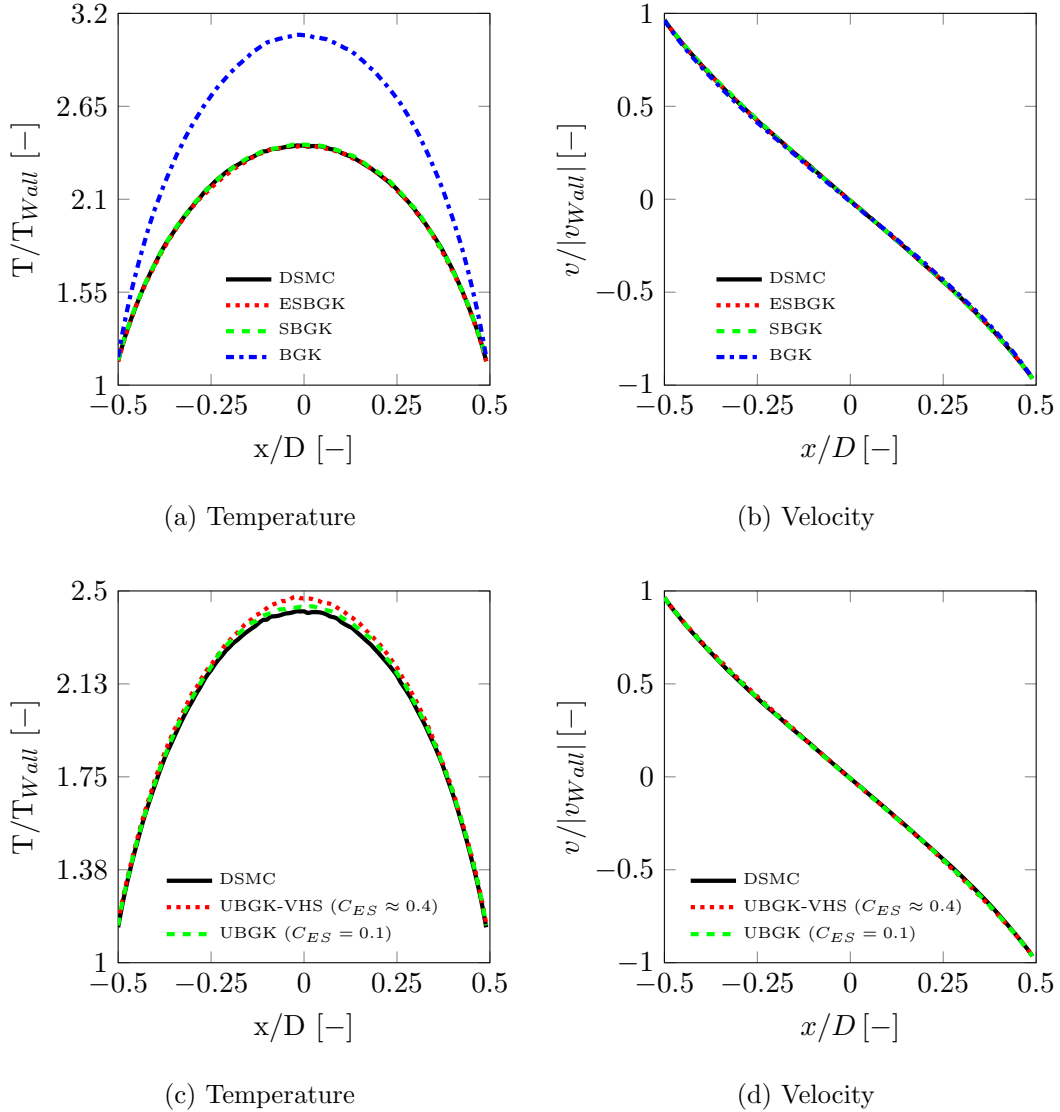


FIG. 3. (a) & (b): Velocity and temperature profiles of high wall velocity Couette flow ($Kn \approx 0.014$) using different BGK models. (c) & (d): Velocity and temperature profiles of high wall velocity Couette flow ($Kn \approx 0.014$) using the UBGK method with different C_{ES} .

solution for $C_{ES} = 0$ where the UBGK model reduces to the SBGK model. Nevertheless, this shows the disadvantage of the UBGK method: it is not clear how to choose the appropriate C_{ES} .

3. High Wall Velocity Case - $Kn \approx 0.14$

The conditions are the same as described in Sec. IV A 2. The only difference is the particle density of $n = 1.29438 \cdot 10^{19} \text{ 1/m}^3$, which leads to a Knudsen number of $Kn \approx 0.14$.

Comparison of DSMC and particle based BGK models

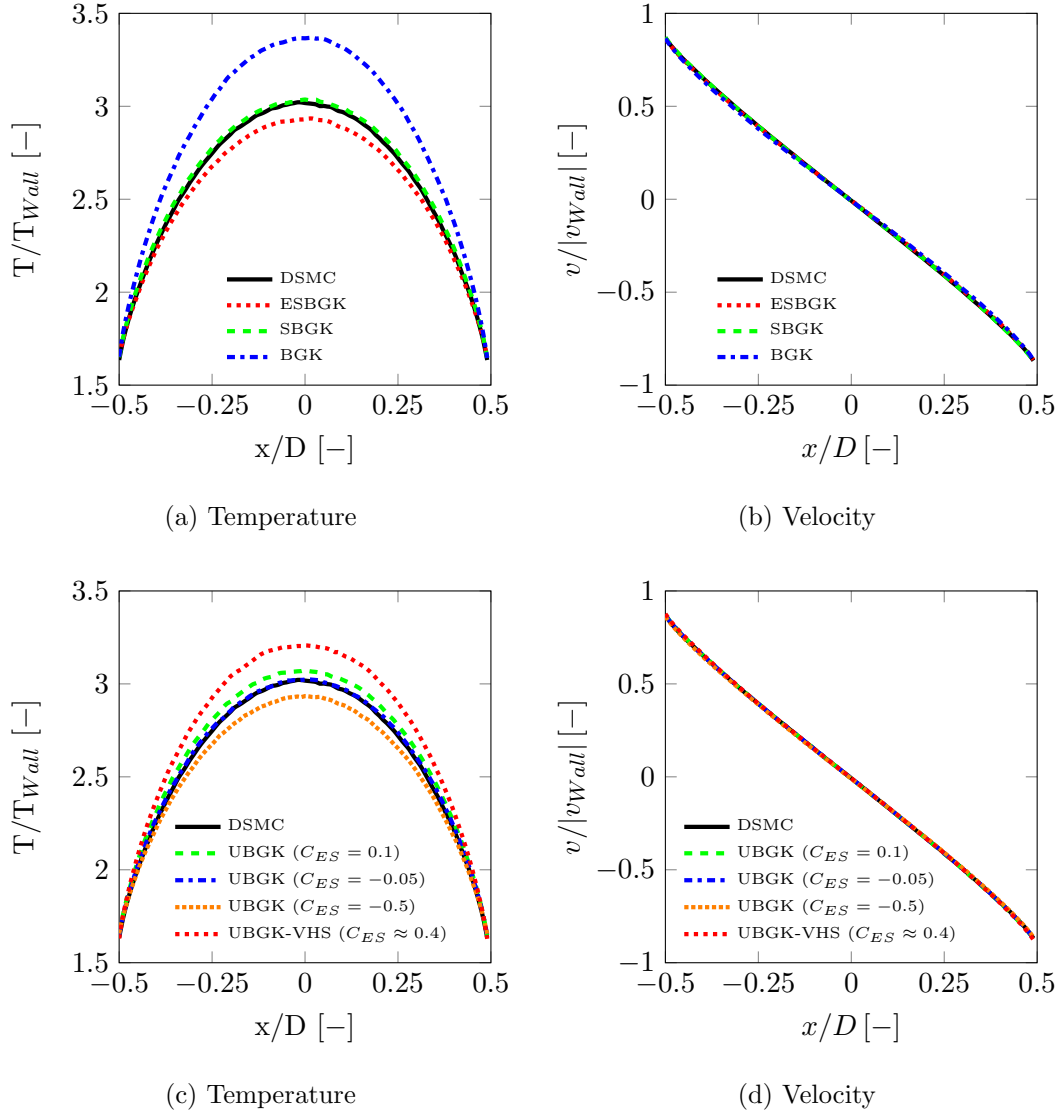


FIG. 4. (a) & (b): Velocity and temperature profiles of high wall velocity Couette flow ($Kn \approx 0.14$) using different BGK models. (c) & (d): Velocity and temperature profiles of high wall velocity Couette flow ($Kn \approx 0.14$) using the UBGK method with different C_{ES} .

Therefore, this case is not in the continuum regime. The temperature and velocity profiles between the plates for the different methods are shown in Fig. 4a and 4b. Here, the SBGK method shows good agreement with the DSMC results, whereas the BGK method overestimates and the ESBGK method underestimates the resulting temperature. Fig. 4c and 4d show additionally an advantage of the UBGK method: the UBGK results can be tuned to match the DSMC results with $C_{ES} = -0.05$ in the non-continuum regime.

Comparison of DSMC and particle based BGK models

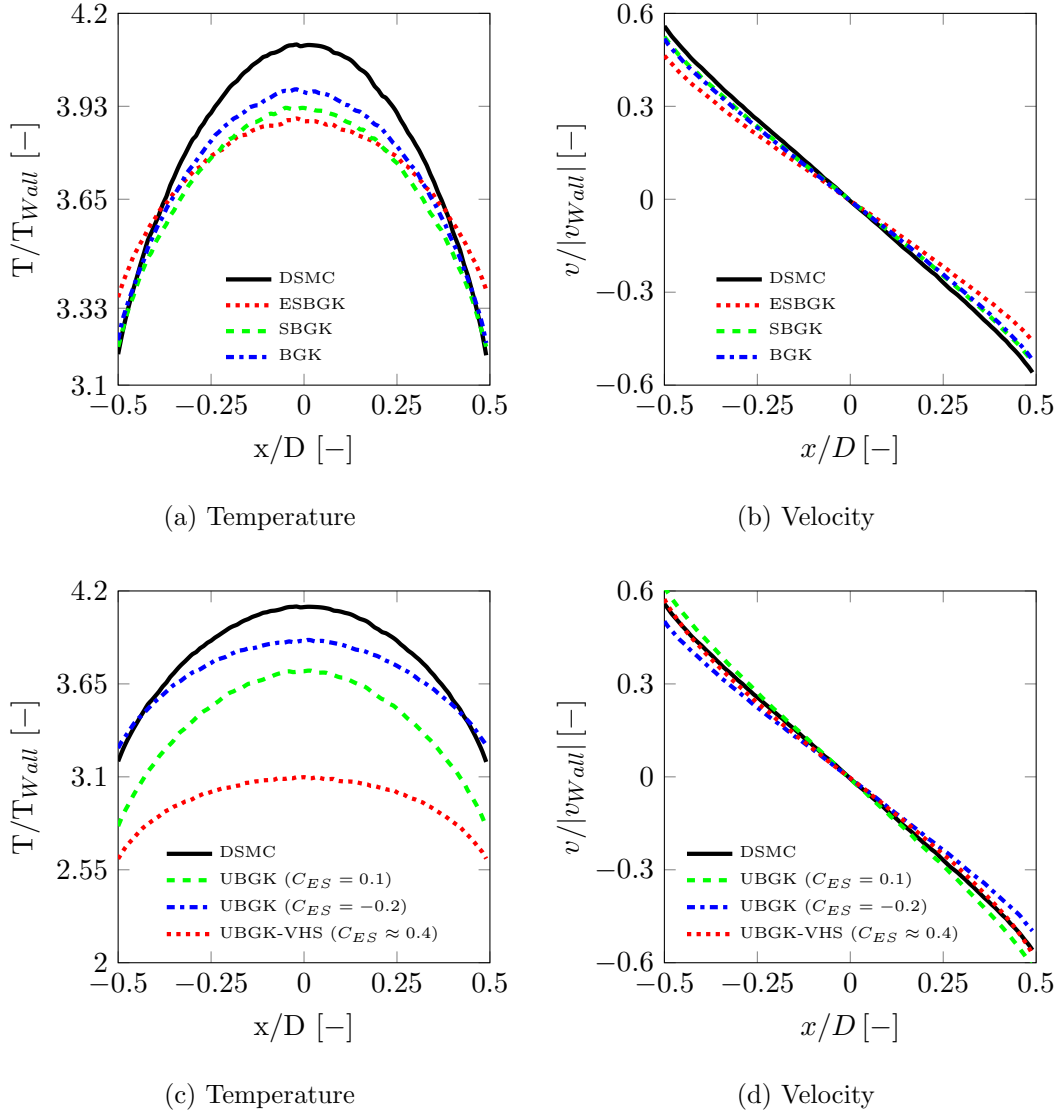


FIG. 5. (a) & (b): Velocity and temperature profiles of high wall velocity Couette flow ($Kn \approx 1.4$) using different BGK models. (c) & (d): Velocity and temperature profiles of high wall velocity Couette flow ($Kn \approx 1.4$) using the UBGK method with different C_{ES} .

4. High Wall Velocity Case - $Kn \approx 1.4$

Finally, the Knudsen number is changed to $Kn \approx 1.4$. In such a rarefied condition, none of the BGK methods is able to reproduce the DSMC results as shown in Fig. 5a-5d. Even the UBGK method is not capable to reproduce the correct values with the constrained $C_{ES} \in [-0.5, 1)$.

	v_∞ [ms ⁻¹]	T_∞ [K]	n_∞ [m ⁻³]	Kn_∞
Set 1	1502.57	13.3	$3.715 \cdot 10^{20}$	≈ 0.033
Set 2	1502.57	13.3	$1.115 \cdot 10^{21}$	≈ 0.011

TABLE II. Inflow conditions of 70° cone test case.

B. 70° Blunted Cone

The 70° blunted cone described in Allegre et al.³¹ is chosen to compare the different BGK models with DSMC. The UBGK model was not used in this investigation. As discussed in Sec. II A 3 it is not clear how to choose C_{ES} for such complex applications. All simulations were carried out for Argon with the inflow conditions of Table II. The angle of attack is set to $\alpha = 0^\circ$. The simulations were performed in 3D to compare the 3D performance between the BGK models and DSMC. All simulations (DSMC as well as all BGK) are performed on the same coarse simulation mesh with 325200 cells. As described in paragraph IV A, an octree method is used in DSMC to resolve the mean free path²⁹. The same octree method is used to subdivide the cells for the BGK methods. Only a certain number of particles per cell form a subcell in the BGK methods to increase the spatial resolution. The points {A,B,C,D} in Fig. 11a correspond to the points in the following line plots.

1. Set 1

Set 1 is a rarefied test case with a Knudsen number of $Kn \approx 0.033$. To resolve the mean free path and the collision frequency in the 3D DSMC simulation a particle number of $N_{DSMC} = 2.2 \cdot 10^7$ and a time step of $\Delta t_{DSMC} = 1 \cdot 10^{-7}$ s are necessary.

The BGK method has similar requirements as the CFD method. The time step can be found using a classic Courant-Friedrichs-Lewy condition with the stream velocity and the speed of sound as described in Mirza et al.⁷. To resolve the temperature and velocity gradients a certain number of cells is required. Additionally, a certain number of particles per cell is required to represent the moments of the distribution function.

Here, the energy conservation scheme becomes crucial. While the energy conservation scheme of Gallis and Torczynski¹³ shows good results with at least 7 to 10 particles per cell, the energy conservation of Burt and Boyd⁸ requires significantly more particles per cell. The

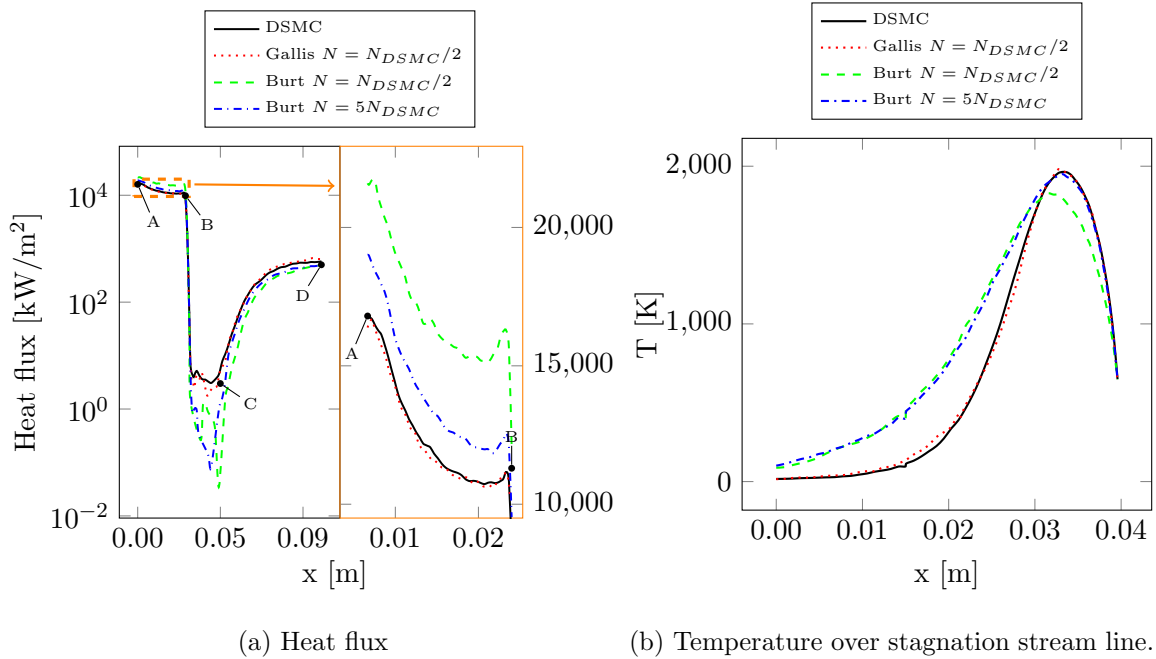


FIG. 6. Cone Set 1 using ESBGK with different energy conservation methods. a: Heatflux plot with magnification of the shield front region. The points {A,B,C,D} correspond to the points depicted in Fig. 11a. b: Comparison of the temperature (shock structure) plot over the stagnation stream line between different models. Particle number and time step for DSMC: $N_{DSMC} = 2.2 \cdot 10^7$, $\Delta t_{DSMC} = 1 \cdot 10^{-7}$ s. Time step for the ESBGK model: $\Delta t = \Delta t_{DSMC}$.

comparison of the ESBGK method with the different energy conserving schemes is shown in Fig. 6.

While the scheme of Gallis compares well with DSMC for the shock profile as well as heat flux on the surface with half the particles, the Burt scheme requires as many as five times more particles than DSMC to produce similar results. It is expected that the shock structure as well as the heat flux will also match the DSMC results with the Burt scheme if the particle number is further increased. However, the particle number was not further increased due to the computational effort and the fact that a similar behavior was already shown in Tumuklu et al.¹⁰. Therefore, it is recommended to use the Gallis scheme for the ESBGK case as is done in the following simulation.

The interpretation of the results for the energy conservation in the SBGK case is less obvious. As shown in Fig. 7, the Gallis scheme matches the shock profile very well and needs much less particles than the Burt scheme to converge. However, the Gallis scheme

underestimates the heat flux on the surface. One possible reason for this behavior and the difference to the ESBGK scheme is that the SBGK model produces skewed distribution functions due to the dependence on the third central moment (the heat flux vector). The energy conservation scheme of Gallis uses the whole distribution function including non-relaxing particles, which seems to blur the skeweness of the distribution function too much, resulting in an incorrect heat flux vector. The ESBGK model seems to be more robust due to the fact that it produces non-skewed distribution functions that are symmetric in each direction.

To overcome the problem of the SBGK model, while using moderate particle numbers, a combination of both energy conserving algorithms can be used. Test simulations have shown that the main problem of the Burt approach are cases with one or two relaxing particles per cell. Therefore, it is proposed to use the Gallis scheme if less than three relaxing particles are in the cell and use the Burt scheme otherwise. All further SBGK simulations are done with this combined energy conservation scheme.

Due to these requirements, the required particle numbers can only be halved in the BGK simulations compared with DSMC for this case.

The comparison of the heat flux and pressure in x-direction between the different methods is shown in Fig. 8a and 8b. The SBGK with the combined energy conservation scheme as well as the ESBGK model with the Gallis scheme match the DSMC results very well, whereas the standard BGK model with the Gallis scheme underestimates the heat flux. Fig. 8c shows the temperature plot over the stagnation stream line. The SBGK model agrees with the DSMC results slightly better than the ESBGK model. However, the predicted early onset of the temperature increase using the ESBGK model resulting in a wider temperature profile is less pronounced as expected.

Furthermore, a time step discretization study was conducted for the SBGK and ESBGK model. The results concerning the heat flux and the shock structure of this investigation are shown in Fig. 9a and 9b. Here, the ESBGK model allows greater time steps, probably due to the fact that the same energy conservation method is used independent from the number of relaxing particles in the cell. The heat flux and the shock structure using the ESBGK method match the DSMC results well up to $\Delta t = 4\Delta t_{DSMC}$, whereas the maximum time step for the SBGK method is $\Delta t = 2\Delta t_{DSMC}$.

A comparison of the computational time is shown in Table III. The coarsest discretization

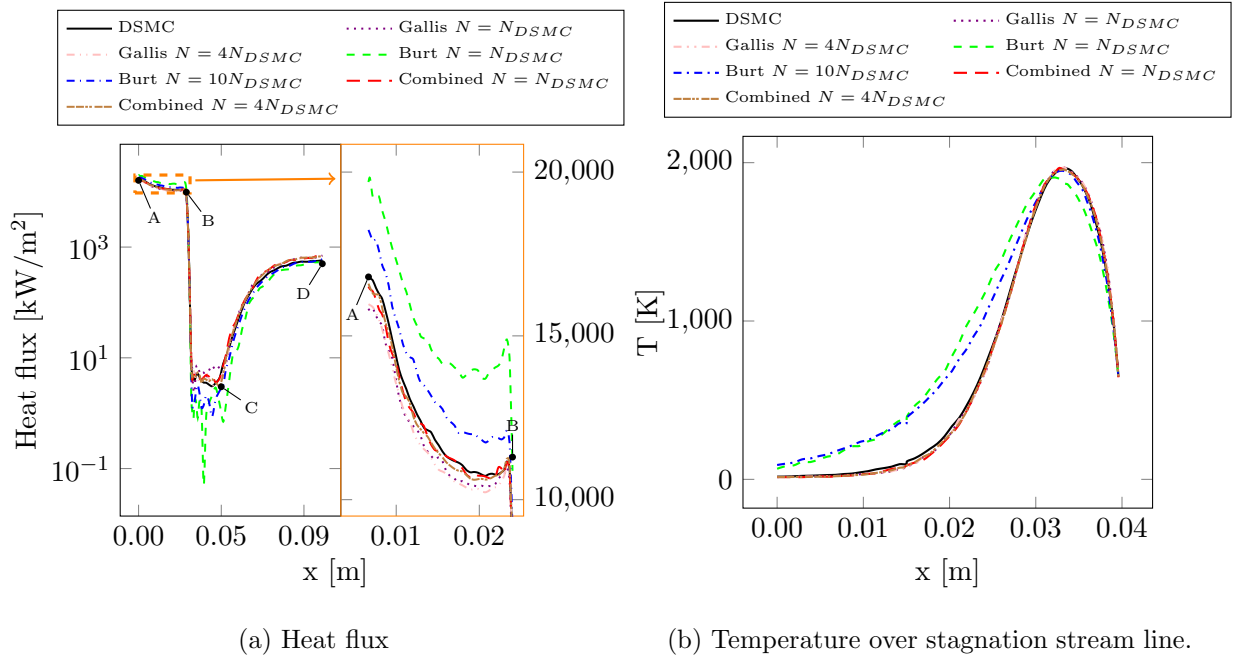


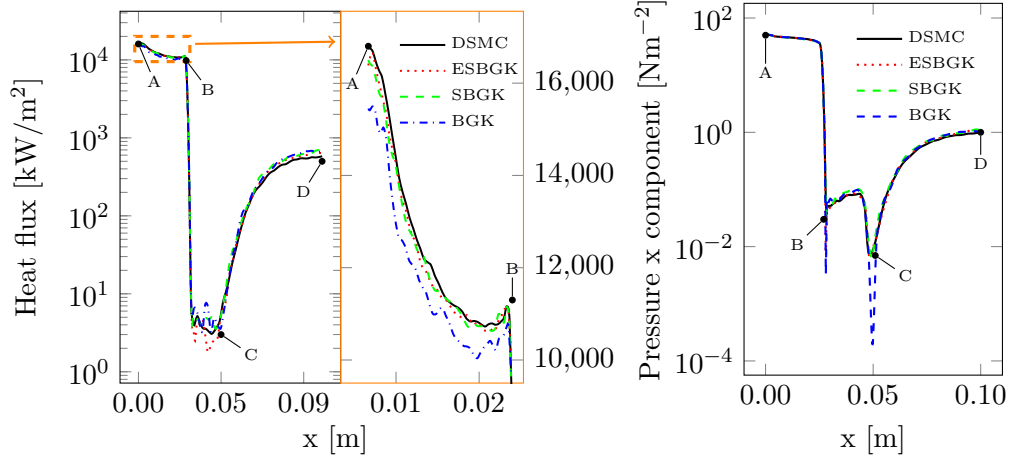
FIG. 7. Cone Set 1 using SBGK with different energy conservation methods. a: Heatflux plot with magnification of the shield front region. The points $\{A,B,C,D\}$ correspond to the points depicted in Fig. 11a. b: Comparison of the temperature (shock structure) plot over the stagnation stream line between different models. Particle number and time step for DSMC: $N_{DSMC} = 2.2 \cdot 10^7$, $\Delta t_{DSMC} = 1 \cdot 10^{-7}$ s. Time step for the ESBGK model: $\Delta t = \Delta t_{DSMC}$.

with acceptable results in terms of the heat flux and shock structure reduces the CPU time by a factor of ≈ 2.5 using the SBGK method and by a factor of ≈ 4.8 using the ESBGK method to reach the same simulation time.

2. Set 2

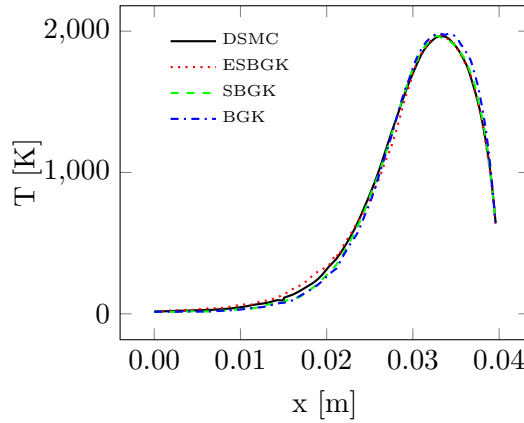
The conditions of Set 2 are given in Table II, where a higher density is assumed with a Knudsen number of $Kn \approx 0.011$. To resolve the mean free path as well as the collision frequency in the 3D DSMC simulation a particle number of $N_{DSMC} = 2.15 \cdot 10^8$ and a time step of $\Delta t_{DSMC} = 5 \cdot 10^{-8}$ s are necessary. The comparison of the heat flux and pressure in x-direction between the different methods is shown in Fig. 10a and 10b. Here, the ESBGK and BGK method are using the energy conservation scheme of Gallis whereas the SBGK method uses the combined scheme. Again, the SBGK as well as the ESBGK model match

Comparison of DSMC and particle based BGK models



(a) Heat flux

(b) Pressure x direction



(c) Temperature over stagnation stream line.

FIG. 8. Cone Set 1. a: Heatflux plot with magnification of the shield front region. b: Pressure on shield in x direction. The points {A,B,C,D} correspond to the points depicted in Fig. 11a. c: Comparison of the temperature (shock structure) plot over the stagnation stream line between different models. Particle number and time step for DSMC: $N_{DSMC} = 2.2 \cdot 10^7$, $\Delta t_{DSMC} = 1 \cdot 10^{-7}$ s. Particle number and time step for the BGK models: $N = N_{DSMC}/2$, $\Delta t = \Delta t_{DSMC}$.

the DSMC results very well, whereas the standard BGK model underestimates the heat flux. All simulations with the different BGK models are performed with eight times less particles $N = N_{DSMC}/8$. Furthermore, the ESBGK and BGK model are using a two times larger time step $\Delta t = 2\Delta t_{DSMC}$ whereas the SBGK model needs the same time step as in DSMC $\Delta t = \Delta t_{DSMC}$. In this case, the shock structure of the ESBGK and SBGK method match the DSMC results equally well as shown in Fig. 11a and 11b and in more detail in Fig. 10c.

Comparison of DSMC and particle based BGK models

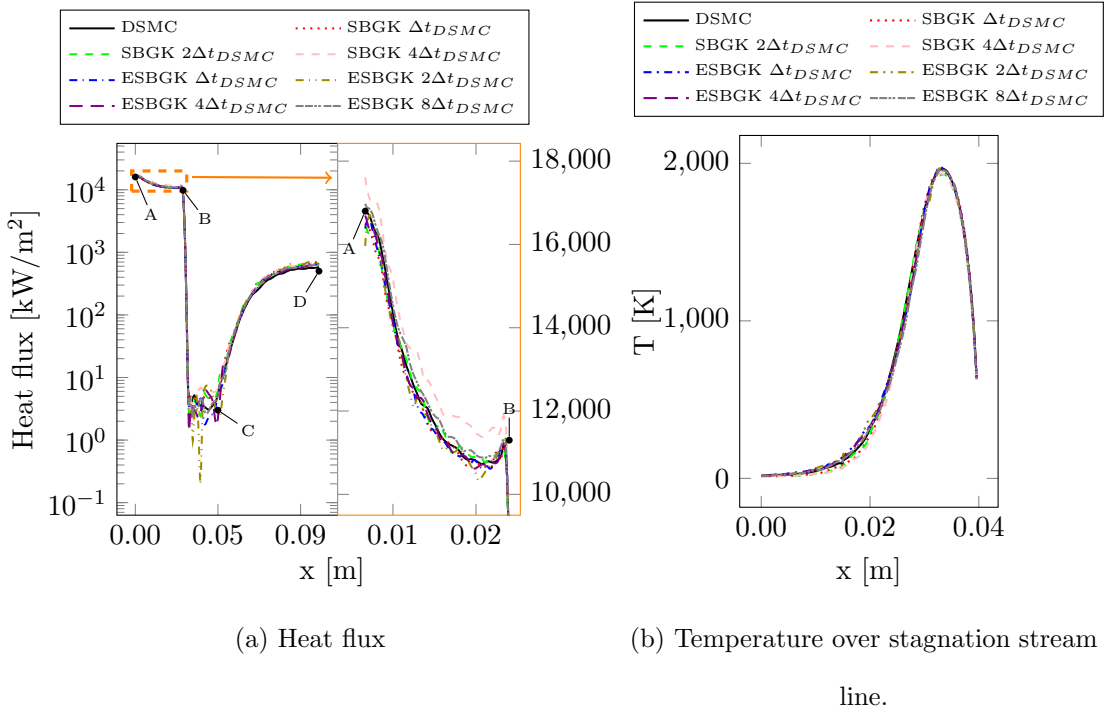


FIG. 9. Comparison of the heat flux and temperature plot over the stagnation stream line between different time step discretizations using ESBGK and SBGK.

	Particle Number N	Time step Δt [s]	CPU Time / 300 iterations [s]	CPU Time / $3 \cdot 10^{-5}$ s Simulation time [s]
DSMC	$2.2 \cdot 10^7$	$1 \cdot 10^{-7}$ s	230	230
ESBGK	$N_{DSMC}/2$	Δt_{DSMC}	152	152
SBGK	$N_{DSMC}/2$	Δt_{DSMC}	175	175
BGK	$N_{DSMC}/2$	Δt_{DSMC}	154	154
SBGK	$N_{DSMC}/2$	$2\Delta t_{DSMC}$	190	95
ESBGK	$N_{DSMC}/2$	$4\Delta t_{DSMC}$	190	47.5

TABLE III. Comparison of CPU time between the different methods for Set 1. The CPU time is the time per node with 24 cores on a Intel Xeon CPU E5-2680 v3.

A comparison of the CPU time is depicted in Table IV. In this case, the BGK methods can substantially save computational time compared with DSMC. For the coarsest discretization with acceptable results in terms of the heat flux and shock structure (ESBGK: $N = N_{DSMC}/8$, $\Delta t = 2\Delta t_{DSMC}$; SBGK: $N = N_{DSMC}/8$, $\Delta t = \Delta t_{DSMC}$) the ESBGK model

Comparison of DSMC and particle based BGK models

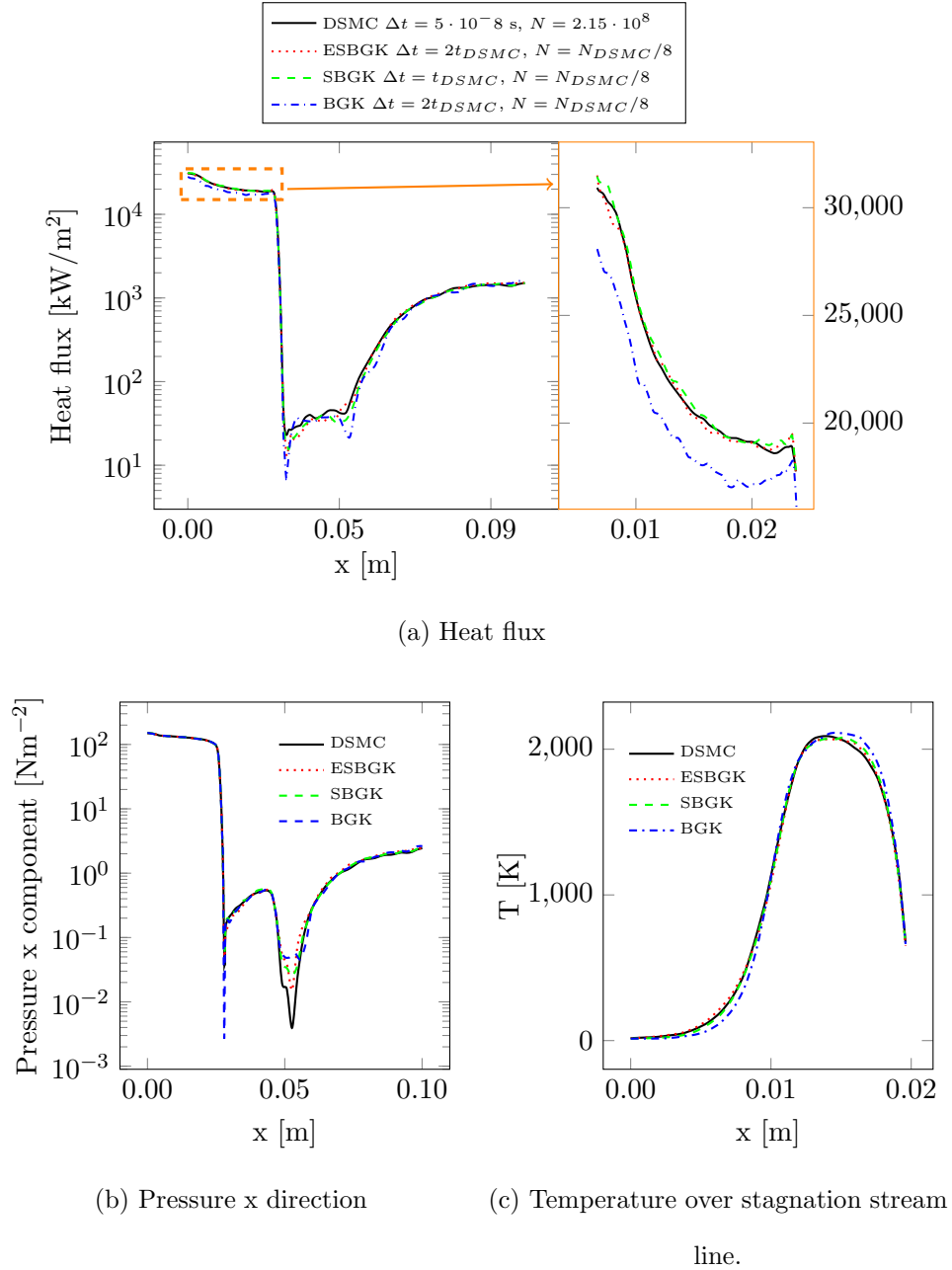


FIG. 10. Comparison of DSMC with the different BGK models. Particle number and time step for DSMC: $N_{DSMC} = 2.15 \cdot 10^8$, $\Delta t_{DSMC} = 5 \cdot 10^{-8}$ s.

reduces the CPU time by a factor of ≈ 17.5 whereas the SBGK reduces the CPU time by a factor of ≈ 8.1 to reach the same simulation time.

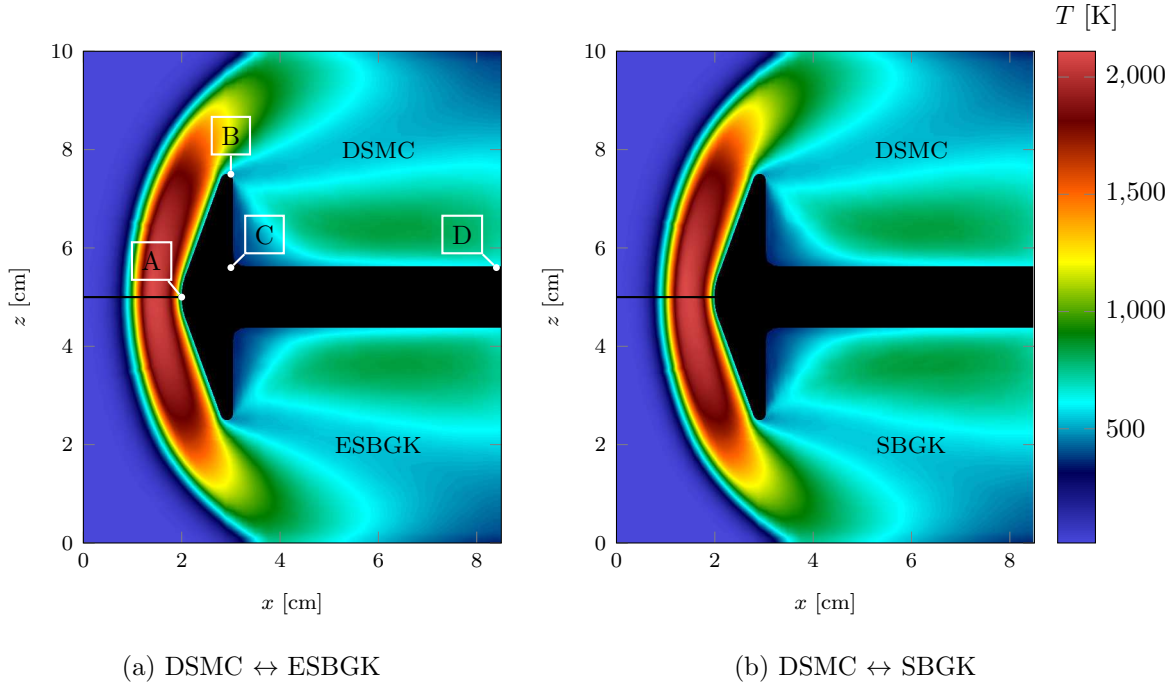


FIG. 11. Temperature plots of ESBGK, SBGK and DSMC to compare the shock structure.

	Particle Number N	Time step Δt [s]	CPU Time / 100 iterations [s]	CPU Time / $1 \cdot 10^{-5}$ s Simulation time [s]
DSMC	$2.15 \cdot 10^8$	$5 \cdot 10^{-8}$ s	820	1640
ESBGK	$N_{DSMC}/8$	$2\Delta t_{DSMC}$	95	95
SBGK	$N_{DSMC}/8$	Δt_{DSMC}	101	202
BGK	$N_{DSMC}/8$	$2\Delta t_{DSMC}$	90	90

TABLE IV. Comparison of CPU time between the different methods for Set 2. . The CPU time is the time per node with 24 cores on a Intel Xeon CPU E5-2680 v3.

V. CONCLUSION AND OUTLOOK

Different ways to sample from an arbitrary velocity distribution function were investigated. Using these methods, it was possible to use the Shakhov BGK and the unified BGK models in an efficient way in the context of particle simulations. Furthermore, different energy conservation scheme for particle based BGK methods were investigated in detail.

The described methods were validated using Couette flow test cases with different wall velocities and Knudsen numbers. It was shown that the SBGK model performs well up to

$Kn = 0.14$ whereas the ESBGK model shows distinct differences to the DSMC simulations in this Knudsen number regime. Furthermore, it was demonstrated that it is possible to capture rarefied flow phenomena using the UBGK model by adapting the additional free parameter of the UBGK model. Nevertheless, it is currently not clear how this additional free parameter should be defined. Therefore, the UBGK model is not useful for practical applications at the moment. Additionally, the computational time of the different BGK methods were compared. Here, it was shown that the investigated sampling methods are not significantly slower than the established method to sample from the ESBGK target function and enables the sampling from the SBGK and UBGK target distribution in an efficient way.

Further on, the BGK, SBGK and ESBGK models were compared with DSMC simulations based on the hypersonic flow around a 70° blunted cone to evaluate the capabilities to capture shock waves. Here, it was shown that the energy conservation scheme is especially crucial for the SBGK method. The ESBGK is more robust concerning the energy conservation and the time step size. Furthermore, the shock profile was not significantly better reproduced by the SBGK model compared with the ESBGK model. However, the heat flux of the SBGK as well as the ESBGK model match the DSMC result very well. It was shown that for a low density case (Case 1), the SBKG model can save up to a factor of ≈ 2.5 and the EBKG model can save up to a factor of ≈ 4.8 CPU time compared with DSMC. With increasing density, the BGK models are able to save significant CPU time compared with DSMC. It was demonstrated that the ESBGK model can save up to a factor of ≈ 17.5 and the SBGK model can save up to a factor of ≈ 8.1 CPU time compared with DSMC for a shock-containing flow problem with a Knudsen number on the order of $Kn \approx 0.011$.

This behavior is especially very interesting for gas flows which cover a wide range of Knudsen numbers including continuum and rarefied gas regions as in nozzle expansion flows, where the coupling of the proposed BGK methods with DSMC is required in order to save computational time. The fact that DSMC and the investigated methods are both cell local Monte-Carlo based particle methods, makes a coupling very simple without the typical problems of hybrid CFD-DSMC methods.

Summarising, the ESBGK model should be preferred over the SBGK model in the presented particle based context. The ESBGK model is able to handle larger time steps than the SBGK model at least until a more robust energy conservation scheme is found for the

SBGK model. Additionally, a general proof exists for the ESBGK model that it always fulfills the H-theorem and it is guaranteed that f^{ES} is positive in each situation.

In the next steps, the described method will be extended to molecules including internal energies. A possible implementation for rotational energies is already given in Burt and Boyd⁸, which was also already extended to vibrational energy modes in Tumuklu et al.¹⁰. Tumuklu et al.¹⁰ showed a similar behavior of the computational efficiency comparing ESBGK and DSMC as described here: the ESBGK method becomes more efficient for an increasing collision frequency compared with DSMC. Therefore, we also expect a reduction of computational time using a BGK method compared to DSMC in small Knudsen number flows including internal energies.

ACKNOWLEDGMENTS

The author gratefully acknowledges the Deutsche Forschungsgemeinschaft (DFG) for funding this research within the project “Partikelverfahren mit Strahlungslöser zur Simulation hochenthalper Nichtgleichgewichts-Plasmen” (project number 93159129). The author also thanks the High Performance Computing Center Stuttgart (HLRS) for granting the computational time that has allowed the execution of the presented simulations.

REFERENCES

- ¹G. A. Bird, *Molecular Gas Dynamics and the Direct Simulation of Gas Flows*, 2nd ed. (Oxford University Press, New York, 1994).
- ²L. Pareschi and S. Trazzi, “Numerical solution of the Boltzmann equation by Time Relaxed Monte Carlo (TRMC) methods,” *International Journal for Numerical Methods in Fluids* **48**, 947–983 (2005).
- ³D. S. Liechty and J. M. Burt, “Extension of the viscous Collision Limiting Direct Simulation Monte Carlo technique to multiple species,” in *AIP Conference Proceedings* (2016) p. 050008.
- ⁴M. H. Gorji and P. Jenny, “An efficient particle Fokker-Planck algorithm for rarefied gas flows,” *Journal of Computational Physics* **262**, 325–343 (2014).

- ⁵M. Pfeiffer and M. Gorji, “Adaptive Particle-Cell algorithm for Fokker-Planck based rarefied gas flow simulations,” *Computer Physics Communications* **213**, 1 – 8 (2017).
- ⁶J. M. Burt and I. D. Boyd, “A Low Diffusion particle method for simulating compressible inviscid flows,” *Journal of Computational Physics* **227**, 4653–4670 (2008).
- ⁷A. Mirza, P. Nizenkov, M. Pfeiffer, and S. Fasoulas, “Three-dimensional implementation of the Low Diffusion method for continuum flow simulations,” *Computer Physics Communications* **220**, 269 – 278 (2017).
- ⁸J. Burt and I. Boyd, “Evaluation of a particle method for the ellipsoidal statistical Bhatnagar-Gross-Krook equation,” in *44th AIAA Aerospace Sciences Meeting and Exhibit* (2006) p. 989.
- ⁹E. Titov, R. Kumar, D. Levin, N. Gimelshein, and S. Gimelshein, “Analysis of different approaches to modeling of nozzle flows in the near continuum regime,” in *AIP Conference Proceedings*, Vol. 1084 (AIP, 2008) pp. 978–984.
- ¹⁰O. Tumuklu, Z. Li, and D. A. Levin, “Particle ellipsoidal statistical Bhatnagar-Gross-Krook approach for simulation of hypersonic shocks,” *AIAA Journal* , 3701–3716 (2016).
- ¹¹S. Chen, K. Xu, and Q. Cai, “A comparison and unification of ellipsoidal statistical and Shakhov BGK models,” *Advances in Applied Mathematics and Mechanics* **7**, 245–266 (2015).
- ¹²P. L. Bhatnagar, E. P. Gross, and M. Krook, “A model for collision processes in gases. I. Small amplitude processes in charged and neutral one-component systems,” *Physical review* **94**, 511 (1954).
- ¹³M. Gallis and J. Torczynski, “Investigation of the ellipsoidal-statistical Bhatnagar-Gross-Krook kinetic model applied to gas-phase transport of heat and tangential momentum between parallel walls,” *Physics of Fluids* **23**, 030601 (2011).
- ¹⁴W. G. Vincenti and C. H. Kruger, *Introduction to physical gas dynamics*, Vol. 246 (Wiley New York, 1965).
- ¹⁵L. H. Holway Jr, “New statistical models for kinetic theory: methods of construction,” *The Physics of Fluids* **9**, 1658–1673 (1966).
- ¹⁶E. Shakhov, “Generalization of the Krook kinetic relaxation equation,” *Fluid Dynamics* **3**, 95–96 (1968).
- ¹⁷H. Struchtrup, “The BGK-model with velocity-dependent collision frequency,” *Continuum Mechanics and Thermodynamics* **9**, 23–31 (1997).

- ¹⁸P. Andries, P. Le Tallec, J.-P. Perlat, and B. Perthame, “The Gaussian-BGK model of Boltzmann equation with small Prandtl number,” *European Journal of Mechanics-B/Fluids* **19**, 813–830 (2000).
- ¹⁹P. Andries and B. Perthame, “The ES-BGK model equation with correct Prandtl number,” in *AIP conference proceedings*, Vol. 585 (AIP, 2001) pp. 30–36.
- ²⁰X. Kun, *Direct modeling for computational fluid dynamics: construction and application of unified gas-kinetic schemes*, Vol. 4 (World Scientific, 2014).
- ²¹C.-D. Munz, M. Auweter-Kurtz, S. Fasoulas, A. Mirza, P. Ortwein, M. Pfeiffer, and T. Stindl, “Coupled Particle-In-Cell and Direct Simulation Monte Carlo method for simulating reactive plasma flows,” *Comptes Rendus Mécanique* **342**, 662–670 (2014).
- ²²M. Gallis and J. Torczynski, “The application of the BGK model in particle simulations,” in *34th Thermophysics Conference* (2000) p. 2360.
- ²³Q. Sun and I. D. Boyd, “Evaluation of macroscopic properties in the direct simulation Monte Carlo method,” *Journal of Thermophysics and Heat Transfer* **19**, 329–335 (2005).
- ²⁴S. Chib and E. Greenberg, “Understanding the Metropolis-Hastings Algorithm,” *The American Statistician* **49**, pp. 327–335 (1995).
- ²⁵W. K. Hastings, “Monte Carlo sampling methods using Markov chains and their applications,” *Biometrika* **57**, 97–109 (1970).
- ²⁶M. Pfeiffer, P. Nizenkov, A. Mirza, and S. Fasoulas, “Direct Simulation Monte Carlo modeling of relaxation processes in polyatomic gases,” *Physics of Fluids* **28**, 027103 (2016).
- ²⁷A. L. Garcia and B. J. Alder, “Generation of the chapman–enskog distribution,” *Journal of Computational Physics* **140**, 66–70 (1998).
- ²⁸R. Kumar, E. Titov, and D. Levin, “Comparison of statistical BGK and DSMC methods with theoretical solutions for two classical fluid flow problems,” in *41st AIAA Thermophysics Conference* (2009) p. 3740.
- ²⁹M. Pfeiffer, A. Mirza, and S. Fasoulas, “A grid-independent particle pairing strategy for DSMC,” *Journal of Computational Physics* **246**, 28–36 (2013).
- ³⁰G. Marsaglia, W. W. Tsang, *et al.*, “The ziggurat method for generating random variables,” *Journal of statistical software* **5**, 1–7 (2000).
- ³¹J. Allègre, D. Bisch, and J. C. Lengrand, “Experimental Rarefied Heat Transfer at Hypersonic Conditions over 70-Degree Blunted Cone,” *Journal of Spacecraft and Rockets* **34**, 724–728 (1997).